

DESY 97-202
October 1997

Event Shape Analysis of Deep Inelastic Scattering Events with a Large Rapidity Gap at HERA

ZEUS Collaboration

Abstract

A global event shape analysis of the multihadronic final states observed in neutral current deep inelastic scattering events with a large rapidity gap with respect to the proton direction is presented. The analysis is performed in the range $5 \leq Q^2 \leq 185 \text{ GeV}^2$ and $160 \leq W \leq 250 \text{ GeV}$, where Q^2 is the virtuality of the photon and W is the virtual-photon proton centre of mass energy. Particular emphasis is placed on the dependence of the shape variables, measured in the γ^* -pomeron rest frame, on the mass of the hadronic final state, M_X . With increasing M_X the multihadronic final state becomes more collimated and planar. The experimental results are compared with several models which attempt to describe diffractive events. The broadening effects exhibited by the data require in these models a significant gluon component of the pomeron.

arXiv:hep-ex/9710027v1 23 Oct 1997

The ZEUS Collaboration

J. Breitweg, M. Derrick, D. Krakauer, S. Magill, D. Mikunas, B. Musgrave, J. Repond, R. Stanek, R.L. Talaga, R. Yoshida, H. Zhang
Argonne National Laboratory, Argonne, IL, USA ^p

M.C.K. Mattingly
Andrews University, Berrien Springs, MI, USA

F. Anselmo, P. Antonioli, G. Bari, M. Basile, L. Bellagamba, D. Boscherini, A. Bruni, G. Bruni, G. Cara Romeo, G. Castellini¹, L. Cifarelli², F. Cindolo, A. Contin, M. Corradi, S. De Pasquale, I. Gialas³, P. Giusti, G. Iacobucci, G. Laurenti, G. Levi, A. Margotti, T. Massam, R. Nania, F. Palmonari, A. Pesci, A. Polini, F. Ricci, G. Sartorelli, Y. Zamora Garcia⁴, A. Zichichi
University and INFN Bologna, Bologna, Italy ^f

C. Amelung, A. Bornheim, I. Brock, K. Coböken, J. Crittenden, R. Deffner, M. Eckert, M. Grothe, H. Hartmann, K. Heinloth, L. Heinz, E. Hilger, H.-P. Jakob, U.F. Katz, R. Kerger, E. Paul, M. Pfeiffer, Ch. Rembser⁵, J. Stamm, R. Wedemeyer⁶, H. Wieber
Physikalisches Institut der Universität Bonn, Bonn, Germany ^c

D.S. Bailey, S. Campbell-Robson, W.N. Cottingham, B. Foster, R. Hall-Wilton, M.E. Hayes, G.P. Heath, H.F. Heath, J.D. McFall, D. Piccioni, D.G. Roff, R.J. Tapper
H.H. Wills Physics Laboratory, University of Bristol, Bristol, U.K. ^o

M. Arneodo⁷, R. Ayad, M. Capua, A. Garfagnini, L. Iannotti, M. Schioppa, G. Susinno
Calabria University, Physics Dept.and INFN, Cosenza, Italy ^f

J.Y. Kim, J.H. Lee, I.T. Lim, M.Y. Pac⁸
Chonnam National University, Kwangju, Korea ^h

A. Caldwell⁹, N. Cartiglia, Z. Jing, W. Liu, B. Mellado, J.A. Parsons, S. Ritz¹⁰, S. Sampson, F. Sciulli, P.B. Straub, Q. Zhu
Columbia University, Nevis Labs., Irvington on Hudson, N.Y., USA ^q

P. Borzemeski, J. Chwastowski, A. Eskreys, J. Figiel, K. Klimek, M.B. Przybycień, L. Zawiejski
Inst. of Nuclear Physics, Cracow, Poland ^j

L. Adamczyk¹¹, B. Bednarek, M. Bukowy, K. Jeleń, D. Kisielewska, T. Kowalski, M. Przybycień, E. Rulikowska-Zarebska, L. Suszycki, J. Zając
Faculty of Physics and Nuclear Techniques, Academy of Mining and Metallurgy, Cracow, Poland ^j

Z. Duliński, A. Kotański
Jagellonian Univ., Dept. of Physics, Cracow, Poland ^k

G. Abbiendi¹², L.A.T. Bauerdick, U. Behrens, H. Beier, J.K. Bienlein, G. Cases¹³, O. Deppe, K. Desler, G. Drews, U. Fricke, D.J. Gilkinson, C. Glasman, P. Göttlicher, T. Haas, W. Hain, D. Hasell, K.F. Johnson¹⁴, M. Kasemann, W. Koch, U. Kötz, H. Kowalski, J. Labs, L. Lindemann, B. Löhr, M. Löwe¹⁵, O. Mańczak, J. Milewski, T. Monteiro¹⁶, J.S.T. Ng¹⁷, D. Notz, K. Ohrenberg¹⁸, I.H. Park¹⁹, A. Pellegrino, F. Pelucchi, K. Piotrkowski, M. Roco²⁰, M. Rohde, J. Roldán, J.J. Ryan, A.A. Savin, U. Schneekloth, F. Selonke, B. Sorrow, E. Tassi, T. Voß²¹, D. Westphal, G. Wolf, U. Wollmer²², C. Youngman, A.F. Żarnecki, W. Zeuner
Deutsches Elektronen-Synchrotron DESY, Hamburg, Germany

B.D. Burow, H.J. Grabosch, A. Meyer, S. Schlenstedt
DESY-IfH Zeuthen, Zeuthen, Germany

G. Barbagli, E. Gallo, P. Pelfer
University and INFN, Florence, Italy^f

G. Maccarrone, L. Votano
INFN, Laboratori Nazionali di Frascati, Frascati, Italy^f

A. Bamberger, S. Eisenhardt, P. Markun, T. Trefzger²³, S. Wölflé
Fakultät für Physik der Universität Freiburg i.Br., Freiburg i.Br., Germany^c

J.T. Bromley, N.H. Brook, P.J. Bussey, A.T. Doyle, N. Macdonald, D.H. Saxon, L.E. Sinclair,
E. Strickland, R. Waugh
Dept. of Physics and Astronomy, University of Glasgow, Glasgow, U.K.^o

I. Bohnet, N. Gendner, U. Holm, A. Meyer-Larsen, H. Salehi, K. Wick
Hamburg University, I. Institute of Exp. Physics, Hamburg, Germany^c

L.K. Gladilin²⁴, D. Horstmann, D. Kçira, R. Klanner, E. Lohrmann, G. Poelz, W. Schott²⁵,
F. Zetsche
Hamburg University, II. Institute of Exp. Physics, Hamburg, Germany^c

T.C. Bacon, I. Butterworth, J.E. Cole, G. Howell, B.H.Y. Hung, L. Lamberti²⁶, K.R. Long,
D.B. Miller, N. Pavel, A. Priniias²⁷, J.K. Sedgbeer, D. Sideris, R. Walker
Imperial College London, High Energy Nuclear Physics Group, London, U.K.^o

U. Mallik, S.M. Wang, J.T. Wu
University of Iowa, Physics and Astronomy Dept., Iowa City, USA^p

P. Cloth, D. Filges
Forschungszentrum Jülich, Institut für Kernphysik, Jülich, Germany

J.I. Fleck⁵, T. Ishii, M. Kuze, I. Suzuki²⁸, K. Tokushuku, S. Yamada, K. Yamauchi, Y. Yamazaki²⁹
Institute of Particle and Nuclear Studies, KEK, Tsukuba, Japan^g

S.J. Hong, S.B. Lee, S.W. Nam³⁰, S.K. Park
Korea University, Seoul, Korea^h

F. Barreiro, J.P. Fernández, G. García, R. Graciani, J.M. Hernández, L. Hervás⁵, L. Labarga,
M. Martínez, J. del Peso, J. Puga, J. Terrón³¹, J.F. de Trocóniz
Univer. Autónoma Madrid, Depto de Física Teórica, Madrid, Spainⁿ

F. Corriveau, D.S. Hanna, J. Hartmann, L.W. Hung, W.N. Murray, A. Ochs, M. Riveline,
D.G. Stairs, M. St-Laurent, R. Ullmann
McGill University, Dept. of Physics, Montréal, Québec, Canada^{a, b}

T. Tsurugai
Meiji Gakuin University, Faculty of General Education, Yokohama, Japan

V. Bashkirov, B.A. Dolgoshein, A. Stifutkin
Moscow Engineering Physics Institute, Moscow, Russia^l

G.L. Bashindzhagyan, P.F. Ermolov, Yu.A. Golubkov, L.A. Khein, N.A. Korotkova,
I.A. Korzhavina, V.A. Kuzmin, O.Yu. Lukina, A.S. Proskuryakov, L.M. Shcheglova³²,
A.N. Solomin³², S.A. Zotkin

Moscow State University, Institute of Nuclear Physics, Moscow, Russia ^m

C. Bokel, M. Botje, N. Brümmer, F. Chlebana²⁰, J. Engelen, E. Koffeman, P. Kooijman,
A. van Sighem, H. Tiecke, N. Tuning, W. Verkerke, J. Vossebeld, M. Vreeswijk⁵, L. Wiggers,
E. de Wolf

NIKHEF and University of Amsterdam, Amsterdam, Netherlands ⁱ

D. Acosta, B. Bylsma, L.S. Durkin, J. Gilmore, C.M. Ginsburg, C.L. Kim, T.Y. Ling,
P. Nylander, T.A. Romanowski³³

Ohio State University, Physics Department, Columbus, Ohio, USA ^p

H.E. Blaikley, R.J. Cashmore, A.M. Cooper-Sarkar, R.C.E. Devenish, J.K. Edmonds,
J. Große-Knetter³⁴, N. Harnew, C. Nath, V.A. Noyes³⁵, A. Quadt, O. Ruske, J.R. Tickner²⁷,
H. Uijterwaal, R. Walczak, D.S. Waters

Department of Physics, University of Oxford, Oxford, U.K. ^o

A. Bertolin, R. Brugnera, R. Carlin, F. Dal Corso, U. Dosselli, S. Limentani, M. Morandin,
M. Posocco, L. Stanco, R. Stroili, C. Voci

Dipartimento di Fisica dell' Università and INFN, Padova, Italy ^f

J. Bulmahn, B.Y. Oh, J.R. Okrasinski, W.S. Toothacker, J.J. Whitmore

Pennsylvania State University, Dept. of Physics, University Park, PA, USA ^q

Y. Iga

Polytechnic University, Sagamihara, Japan ^g

G. D'Agostini, G. Marini, A. Nigro, M. Raso

Dipartimento di Fisica, Univ. 'La Sapienza' and INFN, Rome, Italy ^f

J.C. Hart, N.A. McCubbin, T.P. Shah

Rutherford Appleton Laboratory, Chilton, Didcot, Oxon, U.K. ^o

D. Epperson, C. Heusch, J.T. Rahn, H.F.-W. Sadrozinski, A. Seiden, R. Wichmann, D.C. Williams
University of California, Santa Cruz, CA, USA ^p

O. Schwarzer, A.H. Walenta

Fachbereich Physik der Universität-Gesamthochschule Siegen, Germany ^c

H. Abramowicz³⁶, G. Briskin, S. Dagan³⁶, S. Kananov³⁶, A. Levy³⁶

*Raymond and Beverly Sackler Faculty of Exact Sciences, School of Physics, Tel-Aviv University,
Tel-Aviv, Israel ^e*

T. Abe, T. Fusayasu, M. Inuzuka, K. Nagano, K. Umemori, T. Yamashita

Department of Physics, University of Tokyo, Tokyo, Japan ^g

R. Hamatsu, T. Hirose, K. Homma³⁷, S. Kitamura³⁸, T. Matsushita

Tokyo Metropolitan University, Dept. of Physics, Tokyo, Japan ^g

R. Cirio, M. Costa, M.I. Ferrero, S. Maselli, V. Monaco, C. Peroni, M.C. Petrucci, M. Ruspa,
R. Sacchi, A. Solano, A. Staiano

Università di Torino, Dipartimento di Fisica Sperimentale and INFN, Torino, Italy ^f

M. Dardo

II Faculty of Sciences, Torino University and INFN - Alessandria, Italy^f

D.C. Bailey, C.-P. Fagerstroem, R. Galea, G.F. Hartner, K.K. Joo, G.M. Levman, J.F. Martin, R.S. Orr, S. Polenz, A. Sabetfakhri, D. Simmons, R.J. Teuscher⁵

University of Toronto, Dept. of Physics, Toronto, Ont., Canada^a

J.M. Butterworth, C.D. Catterall, T.W. Jones, J.B. Lane, R.L. Saunders, M.R. Sutton, M. Wing
University College London, Physics and Astronomy Dept., London, U.K.^o

J. Ciborowski, G. Grzelak³⁹, M. Kasprzak, K. Muchorowski⁴⁰, R.J. Nowak, J.M. Pawlak, R. Pawlak, T. Tymieniecka, A.K. Wróblewski, J.A. Zakrzewski

Warsaw University, Institute of Experimental Physics, Warsaw, Poland^j

M. Adamus

Institute for Nuclear Studies, Warsaw, Poland^j

C. Coldewey, Y. Eisenberg³⁶, D. Hochman, U. Karshon³⁶

Weizmann Institute, Department of Particle Physics, Rehovot, Israel^d

W.F. Badgett, D. Chapin, R. Cross, S. Dasu, C. Foudas, R.J. Loveless, S. Mattingly, D.D. Reeder, W.H. Smith, A. Vaiciulis, M. Wodarczyk

University of Wisconsin, Dept. of Physics, Madison, WI, USA^p

A. Deshpande, S. Dhawan, V.W. Hughes

Yale University, Department of Physics, New Haven, CT, USA^p

S. Bhadra, W.R. Frisken, M. Khakzad, W.B. Schmidke

York University, Dept. of Physics, North York, Ont., Canada^a

¹ also at IROE Florence, Italy
² now at Univ. of Salerno and INFN Napoli, Italy
³ now at Univ. of Crete, Greece
⁴ supported by Worldlab, Lausanne, Switzerland
⁵ now at CERN
⁶ retired
⁷ also at University of Torino and Alexander von Humboldt Fellow at DESY
⁸ now at Dongshin University, Naju, Korea
⁹ also at DESY
¹⁰ Alfred P. Sloan Foundation Fellow
¹¹ supported by the Polish State Committee for Scientific Research, grant No. 2P03B14912
¹² supported by an EC fellowship number ERBFMBICT 950172
¹³ now at SAP A.G., Walldorf
¹⁴ visitor from Florida State University
¹⁵ now at ALCATEL Mobile Communication GmbH, Stuttgart
¹⁶ supported by European Community Program PRAXIS XXI
¹⁷ now at DESY-Group FDET
¹⁸ now at DESY Computer Center
¹⁹ visitor from Kyungpook National University, Taegu, Korea, partially supported by DESY
²⁰ now at Fermi National Accelerator Laboratory (FNAL), Batavia, IL, USA
²¹ now at NORCOM Infosystems, Hamburg
²² now at Oxford University, supported by DAAD fellowship HSP II-AUFE III
²³ now at ATLAS Collaboration, Univ. of Munich
²⁴ on leave from MSU, supported by the GIF, contract I-0444-176.07/95
²⁵ now a self-employed consultant
²⁶ supported by an EC fellowship
²⁷ PPARC Post-doctoral Fellow
²⁸ now at Osaka Univ., Osaka, Japan
²⁹ supported by JSPS Postdoctoral Fellowships for Research Abroad
³⁰ now at Wayne State University, Detroit
³¹ partially supported by Comunidad Autonoma Madrid
³² partially supported by the Foundation for German-Russian Collaboration DFG-RFBR
(grant no. 436 RUS 113/248/3 and no. 436 RUS 113/248/2)
³³ now at Department of Energy, Washington
³⁴ supported by the Feodor Lynen Program of the Alexander von Humboldt foundation
³⁵ Glasstone Fellow
³⁶ supported by a MINERVA Fellowship
³⁷ now at ICEPP, Univ. of Tokyo, Tokyo, Japan
³⁸ present address: Tokyo Metropolitan College of Allied Medical Sciences, Tokyo 116, Japan
³⁹ supported by the Polish State Committee for Scientific Research, grant No. 2P03B09308
⁴⁰ supported by the Polish State Committee for Scientific Research, grant No. 2P03B09208

- ^a supported by the Natural Sciences and Engineering Research Council of Canada (NSERC)
- ^b supported by the FCAR of Québec, Canada
- ^c supported by the German Federal Ministry for Education and Science, Research and Technology (BMBF), under contract numbers 057BN19P, 057FR19P, 057HH19P, 057HH29P, 057SI75I
- ^d supported by the MINERVA Gesellschaft für Forschung GmbH, the German Israeli Foundation, and the U.S.-Israel Binational Science Foundation
- ^e supported by the German Israeli Foundation, and by the Israel Science Foundation
- ^f supported by the Italian National Institute for Nuclear Physics (INFN)
- ^g supported by the Japanese Ministry of Education, Science and Culture (the Monbusho) and its grants for Scientific Research
- ^h supported by the Korean Ministry of Education and Korea Science and Engineering Foundation
- ⁱ supported by the Netherlands Foundation for Research on Matter (FOM)
- ^j supported by the Polish State Committee for Scientific Research, grant No. 115/E-343/SPUB/P03/002/97, 2P03B10512, 2P03B10612, 2P03B14212, 2P03B10412
- ^k supported by the Polish State Committee for Scientific Research (grant No. 2P03B08308) and Foundation for Polish-German Collaboration
- ^l partially supported by the German Federal Ministry for Education and Science, Research and Technology (BMBF)
- ^m supported by the Fund for Fundamental Research of Russian Ministry for Science and Education and by the German Federal Ministry for Education and Science, Research and Technology (BMBF)
- ⁿ supported by the Spanish Ministry of Education and Science through funds provided by CICYT
- ^o supported by the Particle Physics and Astronomy Research Council
- ^p supported by the US Department of Energy
- ^q supported by the US National Science Foundation

1 Introduction

At HERA a class of neutral current (NC) deep inelastic scattering (DIS) events has been observed which is characterized by a large rapidity gap (LRG) between the proton beam direction and a multi-particle final state [1, 2]. The Q^2 dependence of the LRG event fraction points to a leading twist production mechanism. The rate of LRG events is most commonly accounted for by introducing “diffractive” processes, which proceed via the t-channel exchange of a colour singlet object with quantum numbers of the vacuum, called the pomeron (\mathbb{P}). However, the nature of the pomeron is at present far from clear. Ingelman and Schlein [3] assumed that the pomeron emitted from the proton behaves like a hadron and suggested that it could have a partonic substructure which could be probed by a hard scattering process. The UA8 experiment at CERN later observed events containing two high- p_T jets in $\bar{p}p$ interactions which were tagged with leading protons (or antiprotons). This observation was explained in terms of a partonic structure in the pomeron [4].

Jet production in LRG events at HERA in the photoproduction regime [5] and the pattern of scaling violations in diffractive DIS [6] led to the conclusion that in order to interpret the data within the Ingelman-Schlein approach, the pomeron must have a high gluon content.

Various models for diffractive scattering can be used to describe the hadronic final state in LRG events [7]. The theoretical predictions range from a calculation of gluon pair exchange [8, 9], to a phenomenological description of pomeron quark and gluon densities [10, 11] and to a boson-gluon fusion scheme, where the resulting quark pair evolves into a colour singlet state [12, 13]. Recently, calculations for two- and three-jet production in DIS rapidity gap events have been presented, in which a scalar pomeron is considered to have a pointlike coupling to quark and gluon pairs [14].

In order to obtain a deeper understanding of multihadronic final states with a large rapidity gap, we study shape variables in the centre of mass frame of the observed hadronic system (of mass M_X), interpreting this as the $\gamma^* - \mathbb{P}$ c.m. system, and investigate their dependence upon M_X . This is in analogy with the studies of shape variables in e^+e^- annihilation as a function of \sqrt{s} [15] and to those which led to the interpretation of three-jet events as a consequence of gluon bremsstrahlung [16, 17, 18, 19]. It has also been applied to the dependence of fixed target antineutrino data as a function of W [20].

2 Experimental setup

The data presented here, taken with the ZEUS detector at HERA in 1994, correspond to a luminosity of $2.57 \pm 0.04 \text{ pb}^{-1}$. HERA operated with 153 colliding bunches of 820 GeV protons and 27.5 GeV positrons. Additional unpaired positron and proton bunches circulated, which were used to determine beam related backgrounds.

A description of the ZEUS detector can be found in [22, 21]. The components used in this analysis are briefly discussed here. The uranium-scintillator calorimeter (CAL) [23] covers 99.7% of the total solid angle. It consists of the forward calorimeter (FCAL) covering the range in pseudorapidity¹ $4.3 < \eta < 1.1$, the barrel calorimeter (BCAL) covering $1.1 < \eta <$

¹The ZEUS coordinate system is defined as right-handed with the Z axis pointing in the proton beam direction, and the X axis horizontal, pointing towards the centre of HERA. The pseudorapidity is defined as $\eta = -\ln(\tan \frac{\theta}{2})$, where θ is the polar angle with respect to the proton direction.

-0.75 and the rear calorimeter (RCAL) covering $-0.75 < \eta < -3.8$. Each calorimeter part is segmented into electromagnetic (EMC) and hadronic (HAC) sections. Each section is further subdivided into cells of typically $5 \times 20 \text{ cm}^2$ ($10 \times 20 \text{ cm}^2$ in the RCAL) for the EMC and $20 \times 20 \text{ cm}^2$ for the HAC sections. Under test beam conditions the calorimeter has an energy resolution of $\sigma/E = 18\%/\sqrt{E(\text{GeV})}$ for electrons and $\sigma/E = 35\%/\sqrt{E(\text{GeV})}$ for hadrons. The timing resolution of a calorimeter cell is less than 1 ns for energy deposits greater than 4.5 GeV. In order to minimize the effects of noise due to the uranium radioactivity on the energy measurements all EMC(HAC) cells with an energy deposit of less than 60(110) MeV are discarded from the analysis.

The tracking system consists of a vertex detector (VXD) [24], a central tracking chamber (CTD) [25], and a rear tracking detector (RTD) [26, 21] enclosed in a 1.43 T solenoidal magnetic field. The interaction vertex is measured with a typical resolution along and transverse to the beam direction of 0.4 cm and 0.1 cm respectively.

The position of positrons scattered at small angles with respect to the positron beam direction is measured using the small angle rear tracking detector (SRTD) which is attached to the front face of the RCAL. The SRTD [27] consists of two planes of scintillator strips, each one 1 cm wide and 0.5 cm thick, arranged in orthogonal directions and read out via optical fibers and photo-multiplier tubes.

The luminosity is measured via the Bethe-Heitler process, $ep \rightarrow e\gamma p$, using a lead-scintillator calorimeter (LUMI) [28] which accepts photons at angles ≤ 0.5 mrad with respect to the positron beam direction and is located at $Z = -107$ m.

3 Reconstruction and kinematic variables

The kinematic variables used to describe deep inelastic ep scattering

$$e(k) + p(P) \rightarrow e(k') + X$$

are the following:

the negative squared four-momentum transfer carried by the virtual photon

$$Q^2 = -q^2 = -(k - k')^2,$$

the Bjorken x variable

$$x = \frac{Q^2}{2P \cdot q},$$

the fractional energy transfer to the hadronic final state

$$y = \frac{P \cdot q}{P \cdot k},$$

and the square of the centre-of-mass energy of the virtual-photon proton system (γ^*p)

$$W^2 = (q + P)^2 = \frac{Q^2(1-x)}{x} + M_p^2,$$

where M_p is the proton mass.

These variables, only two of which are independent, can be determined either from the scattered positron or from the hadronic system. They can also be determined from a mixed set of variables, the so-called double angle method [29]. In this analysis, the scattered positron method is used because it provides a better resolution in the kinematic range under study. The variables Q^2 and y , calculated from the scattered positron variables, are given by the expressions

$$Q_e^2 = 2E_e E'_e (1 + \cos\theta'_e),$$

and

$$y_e = 1 - \frac{E'_e}{2E_e} (1 - \cos\theta'_e),$$

where E_e is the incident positron energy and E'_e and θ'_e denote the energy and angle, with respect to the proton direction, of the scattered positron.

To identify the neutral current DIS events the quantity δ is also used:

$$\delta = \sum_i (E_i - p_{zi}),$$

where E_i denotes the energy assigned to the signal in calorimeter cell i and $p_{zi} = E_i \cos\theta_i$, θ_i being the polar angle of the cell. The sum is running over all calorimeter cells. For fully contained DIS events, and neglecting detector smearing effects, $\delta = 2 \cdot E_e$.

In order to describe the kinematics of diffractive scattering

$$e(k) + p(P) \rightarrow e(k') + p(P') + X$$

the following two additional variables are introduced: the squared four-momentum transfer at the proton vertex,

$$t = (P - P')^2,$$

whose absolute magnitude is small compared to $Q^2 + M_X^2$ in the diffractive processes selected in this analysis, and x_P , the fraction of the proton momentum carried by the pomeron, defined as

$$x_P = \frac{(P - P') \cdot q}{P \cdot q} = \frac{M_X^2 + Q^2 - t}{W^2 + Q^2 - M_p^2} \simeq \frac{M_X^2 + Q^2}{W^2 + Q^2},$$

where M_X is the mass of the hadronic system.

In addition, the variable β is defined as

$$\beta = \frac{Q^2}{2(P - P') \cdot q} = \frac{x}{x_P} = \frac{Q^2}{M_X^2 + Q^2 - t} \simeq \frac{Q^2}{M_X^2 + Q^2},$$

which can be interpreted as the fraction of the pomeron momentum carried by the struck quark.

4 Trigger and data selection criteria

Events were filtered online by a three level trigger system [21]. At the first level [30], DIS events are selected by requiring a minimum energy deposition in the EMC section of the CAL. The threshold varies between 3.4 GeV (in the RCAL) and 4.8 GeV (in the BCAL). At the second level (SLT), non- ep background is further reduced by using the measured times of energy deposits and the summed energies from the calorimeter. The events are accepted if $\delta_{SLT} \equiv \sum_i E_i(1 - \cos \theta_i) > (24 - 2E_\gamma)$ GeV, where E_i and θ_i are the energies and polar angles of calorimeter cells, and E_γ is the energy deposit measured in the LUMI photon calorimeter. This requirement on δ_{SLT} does not reject events with initial state QED radiation.

The full event information is available at the third level trigger (TLT). Tighter timing cuts as well as algorithms to remove beam halo and cosmic muons are applied. The quantity δ_{TLT} was determined in the same way as δ_{SLT} . The events were required to have $\delta_{TLT} > (25 - 2E_\gamma)$ GeV. Finally, events were accepted if a scattered positron candidate of energy greater than 4 GeV was found. In total 900,853 NC DIS candidates satisfied the above trigger conditions.

DIS events were selected off-line by looking for scattered positron candidates recognized using the pattern of energy deposition in the calorimeter. The efficiency of the positron identification algorithm, as well as the procedures to incorporate information from the SRTD in order to improve the positron energy and scattering angle measurements are thoroughly discussed in our recent publication on the measurement of the proton structure function F_2 [31].

The off-line cuts used to select multihadronic DIS events are the following:

- $E'_e > 8$ GeV.
- $5 \text{ GeV}^2 \leq Q_e^2 \leq 185 \text{ GeV}^2$.
- $y_e \leq 0.95$. This cut removes fake positrons found in the FCAL.
- $35 \text{ GeV} \leq \delta \leq 65 \text{ GeV}$. This cut removes events with large initial state QED radiation and further reduces the background from photoproduction.
- The events are required to have a reconstructed vertex. This cut suppresses beam-gas background.
- Events with a scattered positron impact point in the RCAL inside a box of $26 \text{ cm} \times 26 \text{ cm}$ around the beam pipe are rejected. This guarantees full containment of the shower in the calorimeter.

A total of 294,527 events were selected this way.

The mass of the final state hadronic system, M_X , can be reconstructed from the energy deposited in the calorimeter cells, excluding those assigned to the outgoing positron. This reconstruction is sensitive to calorimeter noise effects. To improve it, especially at low masses, we removed isolated cells with energy below 140 (160) MeV for EMC (HAC) cells. The following formula was used for the mass reconstruction:

$$M_X^{rec} \equiv A_1 \cdot \sqrt{(\sum E)^2 - (\sum p_X)^2 - (\sum p_Y)^2 - (\sum p_Z)^2} + A_0.$$

The coefficients A_0 and A_1 correct for the effects of energy loss in the inactive material and energy deposits below the threshold. Their values, $A_0 = 1.4$ GeV and $A_1 = 1.21$, were determined from the Monte Carlo simulation so as to give the best estimate of the true invariant mass in diffractive events in the kinematic region of the analysis. In this region, the resolution in M_X^{rec} is approximately $\sigma(M_X^{rec})/M_X^{rec} \approx 60\%/\sqrt{M_X^{rec}}$.

Diffractive events are characterized by a small value of M_X . However a simple selection based on M_X^{rec} is not enough to select diffractive events because the non-diffractive background would be too high even at relatively low values of the mass. This is illustrated in Fig. 1b where the $\ln M_X^{2,rec}$ distribution for the DIS sample with and without a forward rapidity gap requirement is presented along with a comparison with non-diffractive Monte Carlo expectations normalized to the integrated luminosity. Therefore, to reduce such background and extend the range of mass, a selection based on the presence of a forward rapidity gap is applied. The following cuts define the final sample for the analysis:

- $\eta_{max}^{rec} \leq 1.8$, where η_{max}^{rec} is defined as the pseudorapidity of the most forward condensate with an energy above 400 MeV. A condensate is an energy deposit in contiguous cells above 200 MeV in the calorimeter. In Fig. 1c the η_{max}^{rec} distribution for the full DIS data sample as well as for that with $7 \leq M_X^{rec} \leq 25$ GeV (see below) is presented along with a comparison with non-diffractive Monte Carlo expectations normalized to the total integrated luminosity.
- $7 \leq M_X^{rec} \leq 25$ GeV. The lower limit rejects events where the phase space for QCD radiation is limited. The upper cut is dictated mainly by the lack of statistics at high masses, a consequence of the η_{max}^{rec} requirement.
- $W \geq 160$ GeV. This cut helps to suppress the non-diffractive DIS background [32].
- more than three condensates. This requirement ensures that an event plane for the hadronic final state X can be determined.

A total of 2748 events are selected by these requirements. This sample is estimated to have a contamination from beam-gas background below 1%, based on the distribution of events in unpaired bunches. The background due to photoproduction is estimated to be less than 3% from Monte Carlo studies. Both backgrounds have been neglected in the analysis.

The resulting reconstructed values of x_P are below 0.01, thus the selected sample is expected to be due to pomeron exchange [33, 34]. The remaining non-diffractive DIS background varies from 5% at the lower end to 10% at the upper end of the mass range defined above (see Fig. 1b). The background calculation has been checked by reweighting the exponential fall-off in the Monte Carlo sample in order to agree with estimates from fits to the data for $\ln M_X^{2,rec} \lesssim 7$ with M_X^{rec} in GeV [35]. The two calculations agree within errors. This contribution will be subtracted on a bin-by-bin basis in the differential event shape distributions.

5 Monte Carlo simulation

Monte Carlo (MC) event simulation is used to correct for detector acceptance and smearing effects. The detector simulation is based on the GEANT program [36] and incorporates our understanding of the detector and the trigger performance.

Events from standard non-diffractive DIS processes with first order electroweak corrections were generated with the HERACLES 4.5 programme [37]. It was interfaced to ARIADNE [38] version 4.08 for modeling the QCD cascade according to the colour dipole model [39] that includes the boson gluon fusion diagram, denoted hereafter by CDMBGF. The fragmentation into hadrons was performed with the Lund fragmentation scheme as implemented in JETSET 7.4 [40].

In order to model the diffractive hadronic final states we have considered various models for the pomeron. POMPYT [10] is a Monte Carlo implementation of factorisable models for high energy diffractive processes, where, within the framework provided by PYTHIA [41], the initial state proton emits a pomeron according to the Donnachie-Landshoff flux [42]. The pomeron constituents take part in a hard scattering process with the virtual photon (see first diagram of Fig. 1a). The quark density in the pomeron is chosen to be of the type $\beta f(\beta) \propto \beta(1 - \beta)$. In POMPYT the final states come from the fragmentation of a $q\bar{q}$ pair, and QCD effects (e.g. QCD Compton, second diagram of Fig. 1a) are approximated by the leading log approximation for parton showering.

RAPGAP [11] represents an improvement over POMPYT in that a gluon density in the pomeron is also considered, thus giving rise to final states produced by a photon gluon mechanism $\gamma^*g \rightarrow q\bar{q}$ (see third diagram in Fig. 1a). In the version we have used, the Streng parameterization for the pomeron flux [43] was used and the quark and gluon densities in the pomeron satisfy the momentum sum rule. Also, QCD effects are better modeled within the colour dipole model [39] as implemented in ARIADNE [38] than by the leading log parton shower approximation. The colour dipole approximation turns out to be exact in the limit of massless quarks for the process of gluon emission from a $q\bar{q}$ pair. First order electroweak corrections are taken into account with the programme HERACLES [37].

A different approach has recently been proposed by VBLY [14]. Exact $\mathcal{O}(\alpha_s)$ calculations of two- and three-jet production in diffractive DIS are performed. The calculations assume that the pomeron is emitted at the proton vertex according to the Donnachie-Landshoff flux factor. The pomeron, assumed to be scalar, is considered to have a pointlike coupling to a quark pair, which may radiate a gluon, giving rise to $q\bar{q}$ or $q\bar{q}g$ final states, or to a gluon pair, leading to $q\bar{q}g$ final states through the fusion of one of the gluons with the photon at the lepton vertex (Fig. 1a). Thus, the two free parameters in the model are the pomeron coupling to quark ($g_{\mathcal{P}q\bar{q}}$) or gluon ($g_{\mathcal{P}g\bar{g}}$) pairs. Two- and three-jet final states are generated using a y_{min} criterion² with the value set to 0.03. The value of the QCD scale parameter is chosen so as to reproduce the values for first order α_s as measured at PETRA. The Lund fragmentation scheme [44] as implemented with its default parameters in JETSET [40] is used.

The RAPGAP and VBLY models are used for correction purposes, since POMPYT gives a much poorer description of the data, as discussed in the next section.

²For any pair ij of partons, $m_{ij}^2 > y_{min}M_X^2$ is required to avoid soft and collinear divergences.

6 Results

6.1 Global shape analysis

In order to study the dependence of the multihadronic final states on M_X , we calculate in the $\gamma^* - \mathcal{P}$ rest frame³ the momentum tensor [45], $M_{\alpha\beta} = \sum_{i=1}^n p_{i\alpha} p_{i\beta}$, where the sum runs over the n particles (condensates) in a final state and $\alpha, \beta = X, Y, Z$. Diagonalizing the symmetric tensor $M_{\alpha\beta}$ yields three axes \vec{n}_k ($k = 1, 2, 3$) which give the orientation of the system together with three eigenvalues $\lambda_k = \sum_{i=1}^n (\vec{p}_i \cdot \vec{n}_k)^2$, which can be normalized, $Q_k = \lambda_k / \sum_{i=1}^n |\vec{p}_i|^2$, such that they satisfy the relation $Q_1 + Q_2 + Q_3 = 1$. By ordering the unit vectors \vec{n}_k with increasing eigenvalues $Q_1 \leq Q_2 \leq Q_3$, one can define the variables sphericity S , the transverse momenta in $\langle p_{T_{in}}^2 \rangle$ and out $\langle p_{T_{out}}^2 \rangle$ of the event plane as follows:

$$S = \frac{3}{2}(Q_1 + Q_2) = \frac{3}{2} \min_{\vec{n}} \frac{\sum_{i=1}^n p_{T_i}^2}{\sum_{i=1}^n p_i^2} \quad (\vec{n} = \vec{n}_3),$$

$$\langle p_{T_{in}}^2 \rangle = \frac{1}{n} \sum_{i=1}^n (\vec{p}_i \cdot \vec{n}_2)^2,$$

$$\langle p_{T_{out}}^2 \rangle = \frac{1}{n} \sum_{i=1}^n (\vec{p}_i \cdot \vec{n}_1)^2,$$

where \vec{n}_3 is the unit vector along the principal axis, the so called sphericity axis, which minimizes the sum of the squared transverse momenta. The event plane is defined by \vec{n}_2 and \vec{n}_3 , while \vec{n}_1 defines the direction perpendicular to the event plane. Isotropic events are characterized by $S \sim 1$ and collimated two-jets by $S \sim 0$. In models with a constant limited transverse momentum, the mean sphericity values are inversely proportional to the c.m. energy.

Alternatively, one can define the thrust [46] axis, denoted by the unit vector \vec{n}_T , as the direction in space which maximizes the longitudinal momenta, with thrust then being defined as

$$T = \max_{\vec{n}} \frac{\sum_{i=1}^n |\vec{p}_i \cdot \vec{n}|}{\sum_{i=1}^n |\vec{p}_i|} \quad (\vec{n} = \vec{n}_T).$$

Since thrust is a quantity linear in the momenta, it is less sensitive to QCD divergences. Isotropic events are characterized by $T \sim 0.5$ while two-jet events tend towards $T \sim 1$.

³Since the outgoing proton is not measured, the pomeron direction cannot be unambiguously determined. However, its transverse momentum is expected to be small. We therefore assume the emitted pomeron to be collinear with the incident proton, carrying a fraction $x_{\mathcal{P}}$ of its momentum.

In Figs. 2 and 3, several observed differential distributions (i.e. uncorrected for detector and acceptance effects) are presented. Monte Carlo studies show that the detector acceptance and resolution do not significantly bias the shape of these distributions.

The observed polar distribution $\frac{dN}{d|\cos\theta_S|}$ of the sphericity axis with respect to the virtual photon direction, for four different M_X^{rec} intervals, is shown in Fig. 2a. In e^+e^- annihilation this distribution is found to be consistent with the form $(1 + \cos^2\theta_S)$ which is generally considered to give experimental evidence of the fermionic nature of quarks [47]. In contrast, the polar distribution of the sphericity axis measured in the c.m. $\gamma^* - \mathbb{P}$ system is much more peaked, and, within the errors, little dependent on M_X^{rec} . This may be interpreted as a consequence of the t-channel quark propagator in Fig. 1a for which the Born cross section is to a good approximation proportional to $(1 - \cos^2\theta_S)^{-1}$.

The observed sphericity and thrust distributions, in the four M_X^{rec} intervals, are shown in Fig. 3. As the c.m. energy of the $\gamma^* - \mathbb{P}$ collision increases, the sphericity (thrust) distribution shrinks towards smaller (larger) values. This is a sign of collimation, i.e. jet formation along the sphericity or thrust axes.

The corrected mean sphericity $\langle S \rangle$, one minus mean thrust $\langle 1 - T \rangle$ and the mean squared transverse momentum of the final state hadrons w.r.t. the sphericity axis $\langle p_T^2 \rangle$, as well as its components in $\langle p_{T_{in}}^2 \rangle$ and out $\langle p_{T_{out}}^2 \rangle$ of the event plane, are shown in Fig. 4 as a function of M_X in the kinematic region $5 \leq Q^2 \leq 185 \text{ GeV}^2$, $160 \leq W \leq 250 \text{ GeV}$ and $\eta_{max} \leq 1.8$. Here η_{max} is defined as the pseudorapidity of the most forward generated particle with an energy above 400 MeV. These results are corrected for all detector effects, using Monte Carlo data passed through the detector simulation and data reconstruction program. The correction factor applied to the measured mean value, $\langle X \rangle_{data}^{meas}$, is given by the ratio $\langle X \rangle_{MC}^{gen} / \langle X \rangle_{MC}^{rec}$, where $\langle X \rangle_{MC}^{gen}$ and $\langle X \rangle_{MC}^{rec}$ are the mean values from the generated and reconstructed Monte Carlo data respectively. $\langle X \rangle_{MC}^{gen}$ is evaluated at M_X and $\langle X \rangle_{MC}^{rec}$ at M_X^{rec} . The correction factors using the RAPGAP and VBLV event generators deviate from unity typically by less than 5%. The errors quoted in this figure include, added in quadrature, systematic uncertainties due to i) model dependences in the correction procedure, ii) the determination of the boost to the $\gamma^* - \mathbb{P}$ c.m. system using double angle or scattered lepton variables, iii) thresholds for the definition of condensates, iv) variations in the mass reconstruction procedure ($A_0 = 0$ and $A_1 = 1.5$ in previous formula for M_X^{rec}) and v) variation of the η_{max}^{rec} cut between 1.6 and 2.0. The systematic error dominates over the statistical.

Correction to the whole η_{max} range is precluded by the fact that the correction becomes model dependent. In fact while the correction factor within the VBLV model is η_{max} independent, in the RAPGAP model it drops to 0.6 at the highest mass bin. We interpret this as a consequence of the different behaviour of the pomeron remnant in the two models. In RAPGAP, the pomeron remnant, a quark or a gluon, follows the proton direction of flight, while in models based on pointlike couplings like VBLV, the partons at the pomeron vertex are produced at larger angles.

The mean values $\langle S \rangle$ and $\langle 1 - T \rangle$ measured in DIS events with a large rapidity gap at HERA (Figs. 4a, 4b) decrease with increasing M_X . This decrease is much slower than what would be expected in a model with constant limited p_T and opposite to isotropic phase space predictions [47]. The mean transverse momentum with respect to the sphericity axis (Fig. 4c) increases with increasing M_X . This growth is in fact mainly due to the transverse momentum component in the event plane, while that out of the event plane remains fairly constant (Fig. 4d). Therefore, the events become planar. The observed features are similar to those in e^+e^- annihilation as

measured by the PLUTO [15] and TASSO [48] collaborations at DORIS and PETRA (see Fig. 4) at centre of mass energies comparable to the present range of M_X . Overall, the broadening effects measured in DIS final states with a large rapidity gap are stronger than those exhibited by e^+e^- annihilation data. However, we note that the η_{max} requirement precludes a model independent conclusion valid for the complete diffractive sample.

6.2 Comparisons with models

In the previous section we have presented evidence that the DIS large rapidity gap multihadronic final states become planar at high masses. POMPYT, for which broadening effects are given by the leading log approximation for gluon bremsstrahlung from the quark lines, does not describe the data. Not only does it fail to reproduce the M_X^{rec} distribution (not shown), but more important, the expected mean values for the event shape variables studied are much lower than the data (see Fig. 4).

In the VBLY approach [14], the two free parameters, $g_{\mathbb{P}qq}$ and $g_{\mathbb{P}gg}$, are directly related to the fraction of final state events coming from the gluon coupling as well as to the total diffractive cross section. This fraction was determined by fitting to a set of observed distributions such as sphericity, thrust, $\langle p_{T_{in}}^2 \rangle$, $\langle p_{T_{out}}^2 \rangle$ and $|\cos\theta_S|$ as well as the β distributions shown in Fig. 2b, all of them plotted in the four mass intervals considered before. The parameters in RAPGAP have been tuned to describe the H1 diffractive structure function F_2^D in [49] and no additional tuning has been attempted in this analysis.

The results of the VBLY fits (solid lines) and the expectations from RAPGAP (dashed lines) are shown in Figs. 2, 3, and 4. The global normalization in Figs. 2 and 3 is determined by the total number of events in the whole mass range $7 < M_X^{rec} < 25$ GeV. Both models give a reasonable description of the data. Some discrepancies are observed in the $|\cos\theta_S|$ distribution in VBLY. Although in the VBLY model the pomeron coupling to quarks and gluons is pointlike, the β distributions, presented in Fig. 2b, are also reasonably described. The observed shape at small β is generated through the coupling of the pomeron to gluon pairs.

RAPGAP with only a quark density in the pomeron (dotted line in Fig. 4) fails to describe the data. Similarly, VBLY with only the pomeron to quark pair coupling cannot describe the shapes of the sphericity, thrust and β distributions (dotted line in Fig. 2 and 3). Note that the POMPYT prediction shown in Fig. 4 is similar to that of VBLY with only the quark pair coupling (not shown in Fig. 4).

The implementation of the hard gluon bremsstrahlung process in the MC models is insufficient to account for the broadening effects observed in the data. Therefore, the need to include either the pomeron to gluon pairs coupling in VBLY or the gluon density in RAPGAP is very clear. The exact fraction of gluon-induced events is model dependent and it is sensitive to the y_{min} and p_T cuts imposed on the LO matrix elements used. However, in both models a significant fraction of gluon-induced events is required to describe the data. In the kinematic range under study, this fraction is 50% for VBLY and 30% for RAPGAP.

7 Conclusions

We have studied global event shapes in large rapidity gap NC DIS events at HERA in the kinematic range $5 \leq Q^2 \leq 185 \text{ GeV}^2$, $160 \leq W \leq 250 \text{ GeV}$ and $\eta_{max} \leq 1.8$. These events are generally interpreted as due to pomeron exchange. We have investigated the dependence of the event shape variables sphericity, thrust and transverse momenta squared in and out of the event plane with M_X , the c.m. energy of the $\gamma^* - \mathbb{P}$ collision. The polar distribution of the sphericity axis is very peaked and little dependent on M_X . We find that with increasing M_X the large rapidity gap events become more collimated and planar. Broadening effects in the DIS final states with a large rapidity gap call for a mechanism in addition to hard gluon bremsstrahlung. This can be achieved in models where the pomeron has a partonic structure by including a gluon density in the pomeron, as in RAPGAP, or through a pointlike coupling of the pomeron to quark and gluon pairs, as in VBLY. A significant gluon component of the pomeron is necessary for the models to describe the data.

Acknowledgments

The strong support and encouragement by the DESY Directorate have been invaluable. The experiment was made possible by the inventiveness and diligent efforts of the HERA machine group. We acknowledge the support of the DESY computing and network services.

The design, construction and installation of the ZEUS detector have been made possible by the ingenuity and dedicated efforts of many people from the home institutes who are not listed here. Their contributions are acknowledged with great appreciation.

We would like to thank J. Vermaseren and F.J. Ynduráin for very valuable discussions.

References

- [1] ZEUS Collab., M. Derrick et al., Phys. Lett. B315 (1993) 481.
- [2] H1 Collab., T. Ahmed et al., Nucl. Phys. B429 (1994) 477.
- [3] G. Ingelman and P. E. Schlein, Phys. Lett. B152 (1985) 256.
- [4] UA8 Collab., R. Bonino et al, Phys. Lett. B211 (1988) 239;
A. Brandt et al, Phys. Lett. B297 (1992) 417.
- [5] ZEUS Collab., M. Derrick et al., Phys. Lett. B356 (1995) 129.
- [6] H1 Collab., C. Adloff et al., DESY 97-158 (1997).
- [7] M.F. McDermott and G. Briskin, Proc. of Future Physics at HERA, Vol. 2, DESY (1996) 691 (and references therein).
- [8] A. Donnachie and P.V. Landshoff, Phys. Lett. B285 (1987) 172.

- [9] N.N. Nikolaev and B.G. Zakharov, *Z. Phys. C* 53 (1992) 331.
- [10] P. Bruni and G. Ingelman, DESY 93-187 (1993), published in the Proceedings of the International Europhysics Conference on High Energy Physics, Marseille, 1993.
- [11] H. Jung, *Comp. Phys. Comm.* 86 (1995) 147.
- [12] W. Buchmueller and A. Hebecker, *Phys. Lett.* B355 (1995) 573.
- [13] A. Edin, G. Ingelman, J. Rathsman, *Phys. Lett.* B366 (1996) 371;
LEPTO 6.5: A. Edin, G. Ingelman, J. Rathsman, DESY 96-057 (1996).
- [14] J. Vermaseren, F. Barreiro, L. Labarga and F.J. Ynduráin, DESY 97-031, FTUAM 96-7, accepted by *Physics Letters B*.
- [15] PLUTO Coll., Ch. Berger et al., *Z. Phys. C*12 (1982) 297.
F. Barreiro, *Fort. der Phys.* 34 (1986) 503.
- [16] TASSO Collab., R. Brandelik et al., *Phys. Lett.* B86 (1979) 243.
- [17] PLUTO Collab., Ch. Berger et al., *Phys. Lett.* B86 (1979) 418.
- [18] MARKJ Collab., D.P. Barber et al., *Phys. Rev. Lett.* 43 (1979) 830.
- [19] JADE Collab., W. Bartel et al., *Phys. Lett.* B91 (1980) 142. PA02-068.
- [20] M. Derrick et al., *Phys. Lett.* B88 (1979) 177.
- [21] ZEUS Collab., The ZEUS Detector, Status Report 1993, DESY 1993.
- [22] ZEUS Collab., M. Derrick et al, *Z. Phys. C*63 (1994) 391.
- [23] A. Andresen et al., *Nucl. Instr. and Meth.* A309 (1991) 101;
A. Caldwell et al., *Nucl. Instr. and Meth.* A321 (1992) 356;
M. Derrick et al., *Nucl. Instr. and Meth.* A309 (1991) 77;
A. Bernstein et al., *Nucl. Instr. and Meth.* A336 (1993) 23.
- [24] C. Alvisi et al., *Nucl. Instr. and Meth.* A305 (1991) 30.
- [25] N. Harnew et al., *Nucl. Instr. Meth.* A279 (1989) 290;
B. Foster et al., *Nucl. Phys. B, (Proc. Suppl.)* 32 (1993) 181;
B. Foster et al., *Nucl. Instr. Meth.* A338 (1994) 254.
- [26] B. Bock et al., *Nucl. Inst. and Meth.* A344 (1994) 335.
- [27] ZEUS Collab., M. Derrick et al., *Z. Phys. C*69 (1996) 607;
A. Bamberger et al., DESY 97-157 (1997).
- [28] J. Andruszków et al., DESY 92-066 (1992).
- [29] S. Bentvelsen et al., *Proc. of Physics at HERA, Vol 1, DESY* (1992) 23.
- [30] W. Smith et al., *Nucl. Inst. and Meth.* A355 (1995) 278.
- [31] ZEUS Collab., M. Derrick et al., *Z. Phys. C*72 (1996) 399.

- [32] ZEUS Collab., M. Derrick et al., *Z. Phys.* C70 (1996) 391.
- [33] ZEUS Collab., J. Breitweg et al., DESY 97-184 (1997).
- [34] K. Golec-Biernat et al., *Phys. Rev.* D56 (1997) 3955.
- [35] J.M. Hernández, PhD thesis, Universidad Autónoma de Madrid. In preparation.
- [36] GEANT 3.13: R. Brun et al., CERN DD/EE/84-1 (1987).
- [37] A. Kwiatkowski, H. Spiesberger and H.J. Möhring, Proc. of the Workshop on Physics at HERA, Vol. 3, DESY (1992) 1294.
- [38] L. Lönnblad, *Comp. Phys. Comm.* 71 (1992) 15 and *Z. Phys.* C65 (1995) 285.
- [39] Y. Azimov, Y. Dokshitzer, V. Khoze and S. Troyan, *Phys. Lett.* B165 (1985) 147;
G. Gustafson, *Phys. Lett.* B175(1986) 453;
B. Andersson et al., *Z. Phys.* C43 (1989) 625.
- [40] T. Sjöstrand, *Comp. Phys. Comm.* 39 (1986) 347;
T. Sjöstrand and M. Bengtsson, *Comp. Phys. Comm.* 43 (1987) 367.
- [41] H.-U. Bengtsson and T. Sjöstrand, *Comp. Phys. Comm.* 46 (1987) 43 and T. Sjöstrand, CERN-TH.6488/92.
- [42] A. Donnachie and P.V. Landshoff, *Phys. Lett.* B191 (1987) 309.
- [43] K.H. Streng, in Proc. of the Workshop “Physics at HERA”, p. 365, ed. R.D. Peccei (Hamburg 1987).
- [44] B. Andersson et al., *Phys. Rep.* 97 (1983) 31.
- [45] J.D. Bjorken and S.J. Brodsky, *Phys. Rev.* D1 (1970) 1416.
- [46] E. Fahri, *Phys. Rev. Lett.* 39 (1977) 1587, S. Brandt et al., *Phys. Lett.* 12 (1964) 57.
- [47] R.F. Schwitters et al., *Phys. Rev. Lett.* 35 (1975) 1320;
G. Hanson et al., *Phys. Rev. Lett.* 35 (1975) 1609;
Ch. Berger et al., *Phys. Lett.* B78 (1978) 176.
- [48] TASSO Collab., M. Althoff et al., *Z. Phys.* C26 (1984) 157.
- [49] H1 Collab., T. Ahmed et al., *Phys. Lett.* B348 (1995) 681.

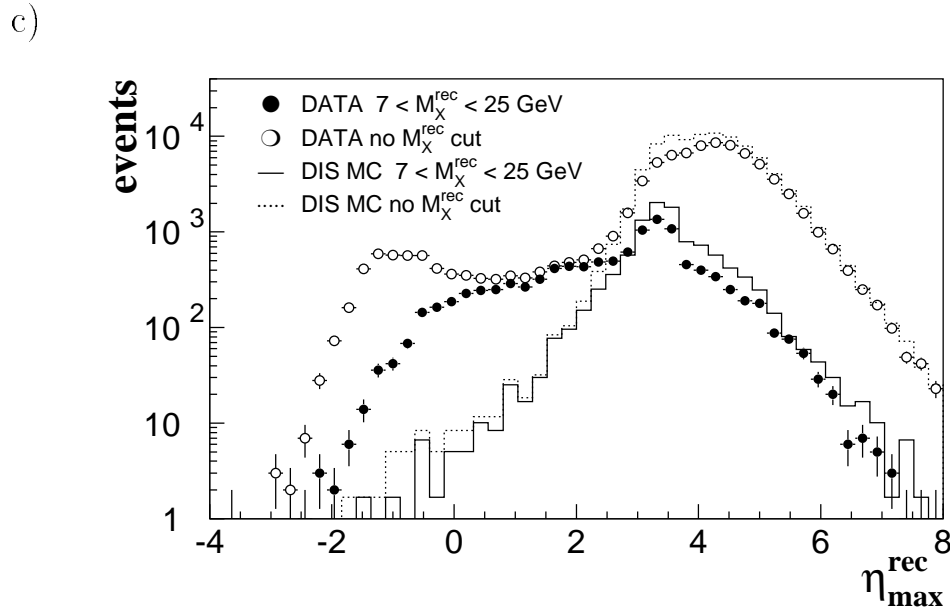
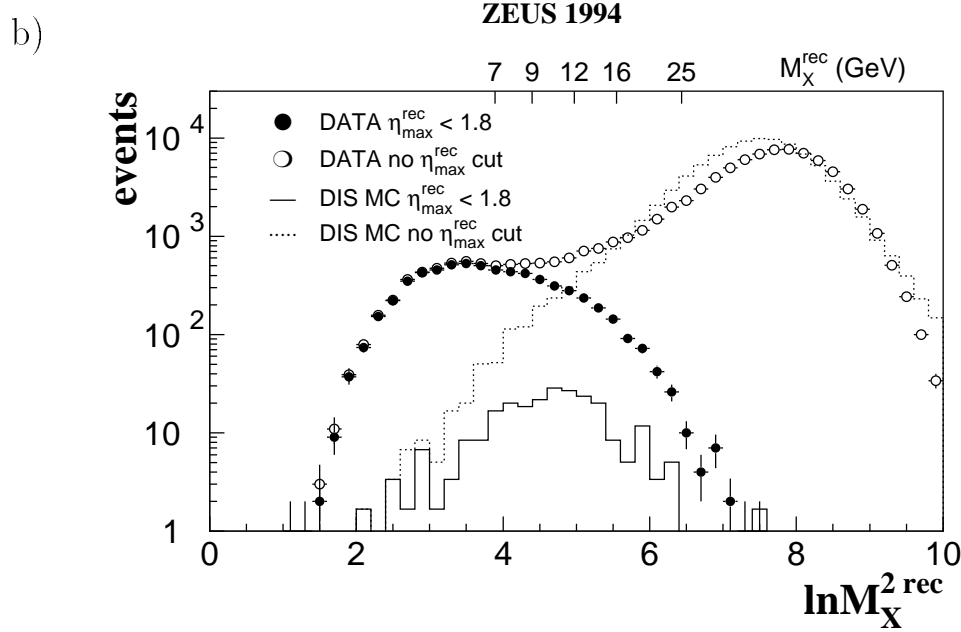
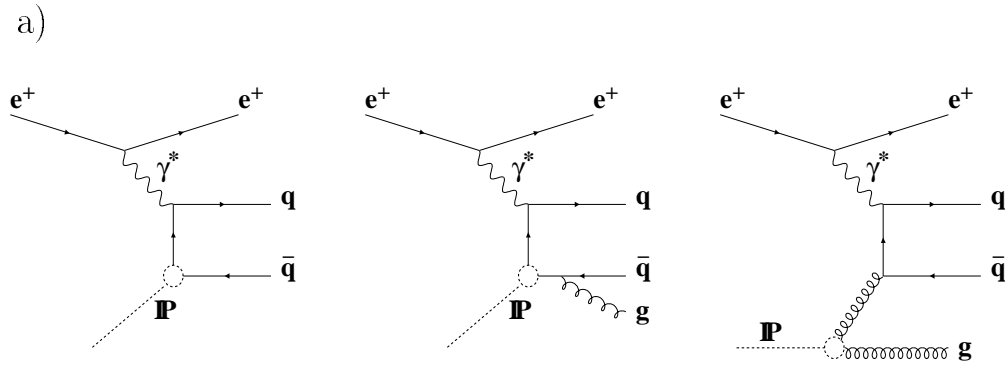


Figure 1: a) Feynman diagrams for processes in the RAPGAP and VBLV models, b) $\ln M_X^{2 \text{ rec}}$ distributions for the complete DIS as well as large rapidity gap samples, along with MC predictions generated within the CDMBGF model and normalized to the integrated luminosity of the data, c) $\eta_{\text{max}}^{\text{rec}}$ distributions for the complete DIS sample as well as for the restricted mass range $7 < M_X^{\text{rec}} < 25 \text{ GeV}$, along with MC predictions as in b).

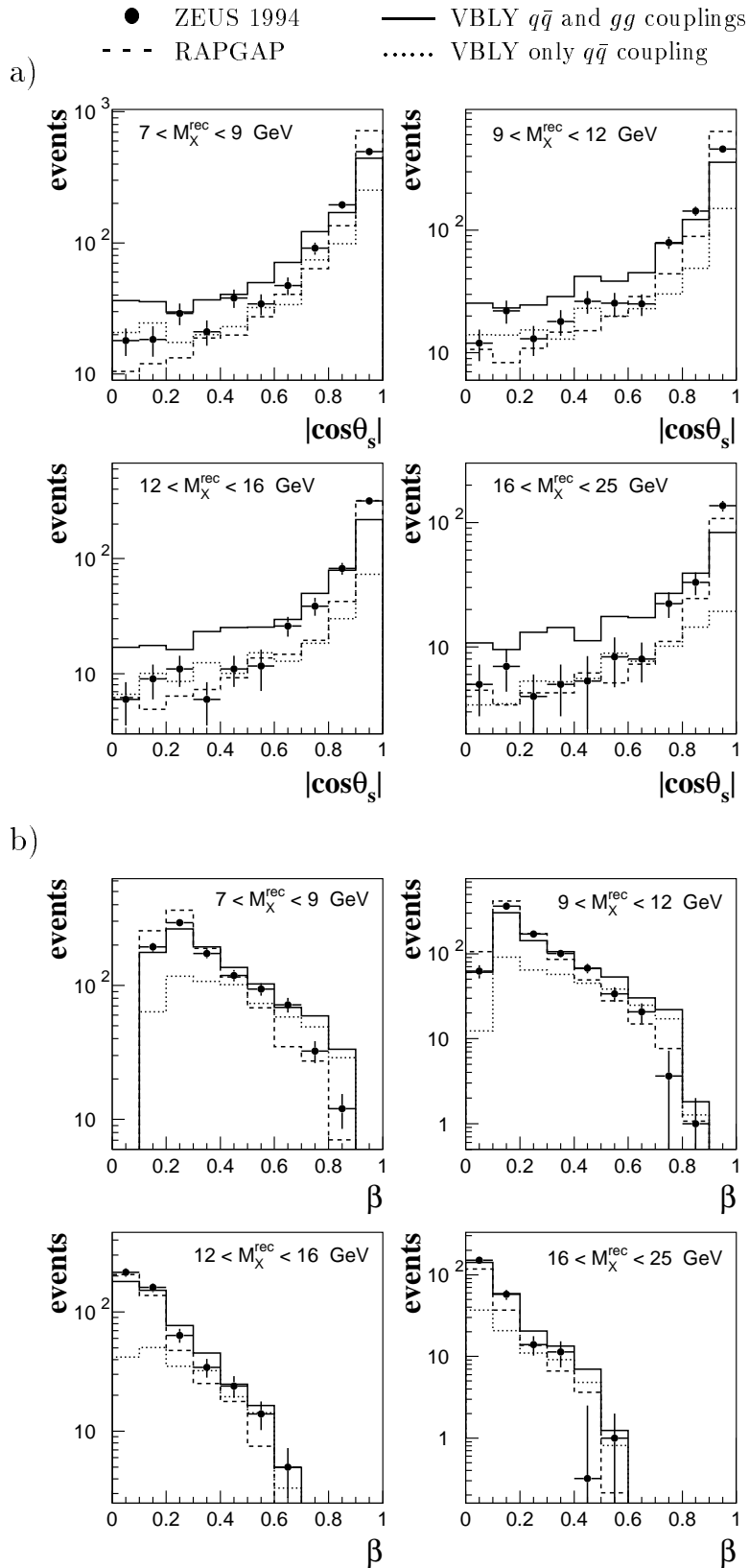


Figure 2: Measured polar distribution of the sphericity axis with respect to the virtual photon direction in the $\gamma^* - IP$ rest frame (a), and measured β distribution (b). The results of the VBLY model are shown as solid lines, with the quark contribution from this model shown as dotted lines. RAPGAP expectations are represented by the dashed lines. The global normalization of the predictions is adjusted so as to match the measured number of events in the whole mass range $7 < M_X^{rec} < 25$ GeV.

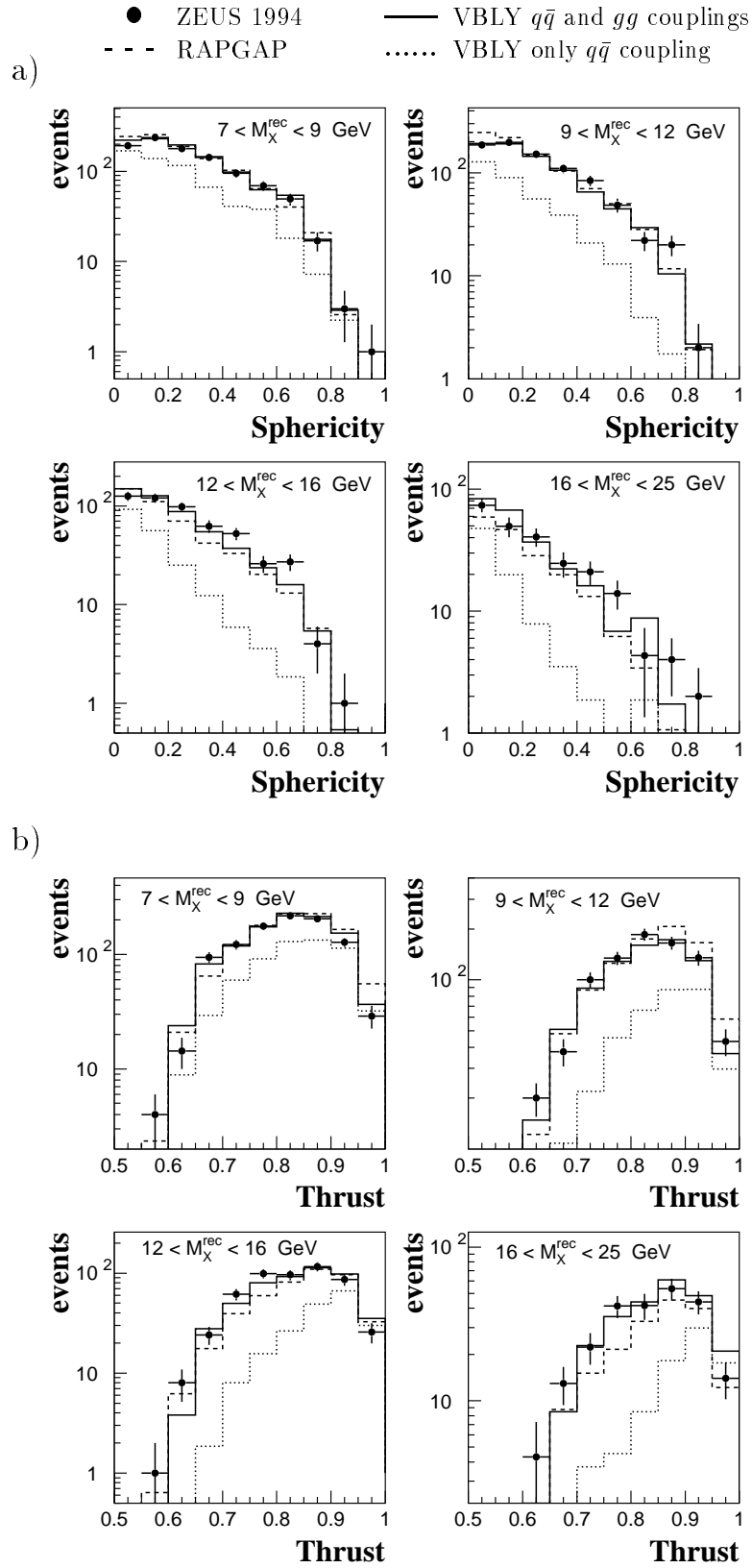


Figure 3: Measured sphericity (a), and thrust distributions (b) for large rapidity gap DIS events in four M_X^{rec} intervals. The results of the VBLY model are shown as solid lines, with the quark contribution from this model shown as dotted lines. RAPGAP expectations are represented by the dashed lines. The global normalization of the predictions is adjusted so as to match the measured number of events in the whole mass range $7 < M_X^{\text{rec}} < 25$ GeV.

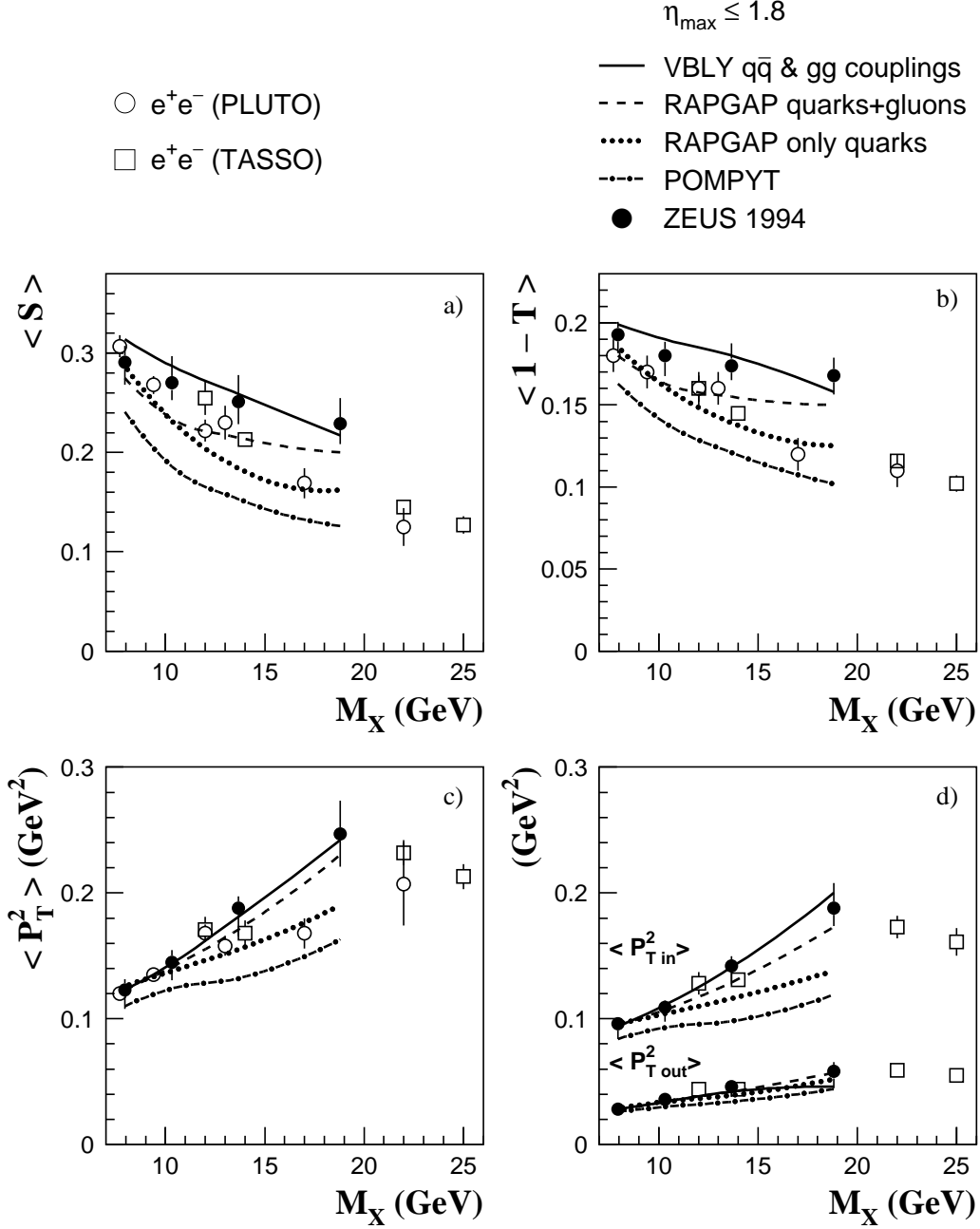


Figure 4: The mean sphericity, one minus mean thrust, mean squared transverse momenta w.r.t. the sphericity axis and its components in and out of the event plane, plotted as a function of M_X . Open dots and squares represent PLUTO and TASSO measurements at DORIS and PETRA, respectively. Black dots represent the ZEUS data corrected for detector effects to the kinematic region $5 \text{ GeV}^2 \leq Q^2 \leq 185 \text{ GeV}^2$, $160 \text{ GeV} \leq W \leq 250 \text{ GeV}$ and $\eta_{\max} \leq 1.8$. Note that the ZEUS data and the predictions from the models are for $\eta_{\max} \leq 1.8$.